MEMS Comb Drive Actuator to Vary Tension and Compression of a Resonating Nano-Doubly Clamped Beam for High-Resolution and High-Sensitivity Mass Detection

Adam Hurst[1], Chou Ying-Chi[1], John Regis[1], Andrew Lie[2], and Adrian Podpirka[3]

Department of Mechanical Engineering, Columbia University
500 W. 120 Street, Room 220 Mudd, New York, NY 10027, USA

Abstract – Micro-electromechanical systems (MEMS) often provide cost effective solutions with rapid response times to many macroscopic engineering enigmas. While MEMS devices offer micro-scale actuation and sensing, nano-electromechanical systems (NEMS) give even greater sensitivity, faster response times, and a larger breadth of applications. Nano-sized resonating beams, specifically, provide promise in ultra-sensitive mass detection and substance sensing. Detection is achieved through the coloration of resonant frequency shifts with the existence of specific environmental conditions. In an effort to increase sensitivity, we have designed a micro-scale comb drive electrostatic actuator. Our MEMS device will have the versatility to load a 10 μm long, 80 nm wide, and 100 nm thick gold/palladium beam with tensile and compressive stresses. The structure is made using a combination of electron beam evaporation of gold and palladium, Reactive Ion Etching (RIE), and 5:1 BHF etchant on a Si-SiO$_2$-Si wafer. A voltage applied to the comb drive will change the compression and tension of the beam. The beam will drive and the resonant frequency will be determined by a magnetomotive technique [13]. A DC voltage along with a sinusoidal current, which is out of phase with the resonating beam, will be applied to comb drive plates in order to keep the structure stable and apply the desired tensile or compressive loading. The device is packaged using an innovative leadless contact approach, which increases stability over time and environment. Potential applications include gas and homeland security bioterrorism sensors.

Index Terms – Electrothermal tuning, thermal time constant, MEMS resonator, NEMS resonator, resonating beam sensor, leadless packaging.

[1] Graduate Student in Mechanical Engineering, Columbia University
[2] Undergraduate Student in Mechanical Engineering, Columbia University
[3] Undergraduate Student in Material Science and Engineering, Columbia University

I. Introduction

Micro-electromechanical systems (MEMS) and nano-electromechanical systems (NEMS) have a wide range of applications from sensors that can detect the finite amounts of organic compounds or gases such as hydrogen. Delving into nano-structures has resulted in the discovery of hypersensitive devices. Nanobeams, for example, experience changes in their lattice structure or mass loading. As classical mechanics

suggests, such changes in beam dimensions or loading causes a resonant frequency shift. Frequency shifts of a nano-scale beam are detected and correlated with the presence of a particular substance. Due to their miniscule size and intricate design, nano-electromechanical systems routinely reach high frequencies on the order of GHz. The fabrication of a resonating beam leaves residual tensile stresses on the beam. It has been discovered that such resonating beams are less sensitive under these tensile loads [13]. Therefore a motivation has risen to load the beam with tensile and compressive stresses in order to further examine beam sensitivity and resonance. The ideal beam loading device is a MEMS actuator.

In this paper we report an intricate design of a MEMS comb drive electrostatic actuator tailored to apply compressive and tensile loads to the doubly clamped NEMS resonating beam on the order of $\approx$ +/- 200 MPa. The structure will work on the application of an electrostatic force from an applied voltage bias.

The research disclosed within this paper describes the properties of the nano-mechanical resonator, the thermal time constant of such a resonator, the design, fabrication and packaging of the comb drive electrostatic actuator to create an adjustable load on the NEMS resonating beam. An innovative leadless packaging system is also disclosed. Numerous applications exist for such resonating beams. Some such applications include but are not limited to bio-terrorism sensors for homeland security issues or gas sensors.

II. Theoretical Background & Design

Hypersensitivity may be achieved when a compressive force is applied to the NEMS beam. In an effort to optimize the sensitivity of NEMS resonating beams, our MEMS electrostatic actuator has been designed to accurately place a compressive and tensile load on the beam. It has been estimated that sensitivity optimization would occur within the load range of $\approx$ +/- 200 MPa. The beam is assumed to be constructed as a composite of gold and palladium. The effective Young's modulus, $E_{eAu/Pd\&Si}$, and density, $\rho_{eAu/Pd\&Si}$, are given by

$$E_{eAu/Pd} = \frac{E_{Au}A_{Au} + E_{Pd}A_{Pd}}{A_{Au} + A_{Pd}}$$
Equation 1 [13]

$$\rho_{eAu/Pd} = \frac{\rho_{Au}A_{Au} + \rho_{Pd}A_{Pd}}{A_{Au} + A_{Pd}}$$
Equation 2 [13]

where A is the area.

Similarly, the composite structure of silicon with evaporated gold and palladium on its surface has an effective Young's modulus, $E_{e,Si,Au/Pd}$ defined by

$$E_{eAu/Pd\&Si} = \frac{E_{eAu/Pd}A_{Au/Pd} + E_{eSi}A_{Si}}{A_{Au/Pd} + A_{Si}}$$
Equation 3 [13]

$$\rho_{eAu/Pd\&Si} = \frac{\rho_{eAu/Pd}A_{Au/Pd} + \rho_{eSi}A_{Si}}{A_{Au/Pd} + A_{Si}}$$
Equation 4 [13]

Applying the classical pressure equation, displayed below, the required

force on the beam is determined, with P representing pressure, *F* as force, and A equaling the cross sectional area of the beam.

$$P = \frac{F}{A_{Au/Pd}}$$
Equation 5 [15]

The beam axial deflection under such a load is calculated through the effective young's modulus and initial beam length, L_0. The axial deflection is given by

$$\Delta L = \frac{\sigma}{E_{Au/Pd}} L_0$$
Equation 6 [5]

These calculations indicate required force and deflection that a MEMS device must create for effective testing. While many appropriate MEMS actuators exist, we determined a comb drive to be the the most effective based on a fabrication and performance analysis.

Our comb drive consists of numerous suspended finger structures. Comb drive electrostatic actuation offers a nearly linear resultant force due to input voltage, which is desirable. Other MEMS devices such as capacitive electrostatic or magneto motive actuators possess non-linear relationships between applied bias and output force or displacement. While such force/voltage relationships can be modeled, the variability in fabrication is very likely to result in inaccuracy between theoretically predicted and actual performance. Such variability is eliminated with the use of a comb drive.

Comb drives actuate motion through an applied voltage between two parallel plates. A lateral attractive force is generated when one grounded finger or plate is surrounded by two additional fingers or plates powered at a high voltage. The electrical field generated between these plates cause equal and opposite attractive forces that prevent snap down while generating a lateral force. The energy in one of these charged parallel plate capacitors is defined by

$$U = \frac{1}{2} \frac{\varepsilon_r \varepsilon_0 A V^2}{d}$$
Equation 7

where U is the energy, ε_0 is the permittivity of free space, ε_r is the relative permittivity, A is area of the face of the plate, V is the applied voltage, and d is the gap between the plates [7]. The derivative of this energy equation with respect to the lateral direction is the generated force in the horizontal direction, which is displayed below.

$$F_x = \frac{\varepsilon_r \varepsilon_0 w V^2}{d}$$
Equation 8

In this instance, w is the width of the parallel plates [7]. The equation above is valid only when the overlap distance is assumed to be considerable in comparison to the other dimensions of the fingers. Figure 1 illustrates the effective comb drive actuation.
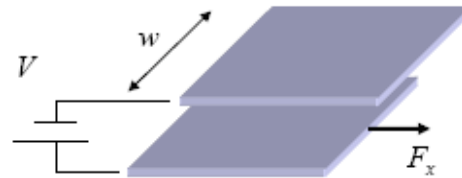
Effective comb drive actuation
Figure 1 [7]

Similar to capacitive plate snap down, comb drives can experience side

instability or snap down between adjacent plates. Side instability can exist if the comb drive does not possess enough rigidity. Comb drives should be dimensioned such that the side instability voltage is significantly outside the operating range. The side instability voltage is defined by

$$V_{SI} = \frac{d^2 k_y}{2\varepsilon_o bn}\left(\sqrt{2\frac{k_x}{k_y} + \frac{y_o^2}{d^2}} - \frac{y_o}{d}\right)$$
Equation 9

where d is the distance between combs, k_y and k_x is a comb drive finger spring constant along the vertical and horizontal axis, respectively, b is the base, n is the number of combs, d is the distance between plates, and y_0 is the initial length of the finger [8].
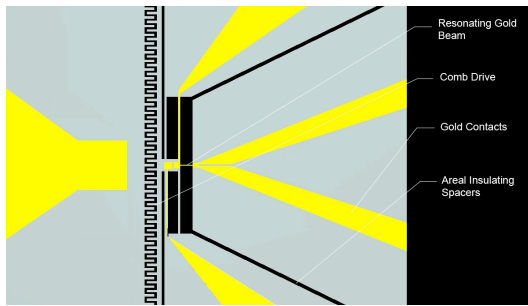

Image of support beams and structure
Figure 2

While effective comb drive electrostatic actuation creates the appropriate forces, such structures must be released from the surface while remaining attached to the wafer. Support beams successfully secure the resonating nano-beam and released comb drive structure to the wafer. These can be viewed in Figure 2 above. Such beams act as springs, deflecting as a result of the force generated by the comb drives. They are assumed to act similar to cantilever beams. These beams can be viewed in the lower and upper sections

of Figure 3 as well. In this application, the effective spring constant, k, of a cantilevered beam is dependent upon the composite Young's modulus, E_e, the base, b, height, h, and length, L of the beam.

$$k_y = \frac{E_e h b^3}{4L^3} = \frac{3E_e I_{yy}}{L^3}$$
Equation 10

$$k_x = \frac{3E_e I_{xx}}{L^3} = \frac{E_e b h^3}{4L^3}$$
Equation 11

Doubly Clamped Nanobeam
Figure 3

The effective spring constant of several identical cantilever beams is defined by

$$k_{eff} = n \cdot k$$
Equation 12

where n is the number of identical cantilever beams supporting the structure and k is the spring constant of one such beam.

The force related with bending such a spring is defined by

$$F_x = k_{eff} \cdot x$$
Equation 13

The vertical deflection of such cantilevered beams used to suspend the comb drive and resonating beam is defined by

$$v(x) = \frac{F}{6E_{eAu/Pd}I}(3x^2L - x^3)$$

Equation 14 [5]

where *v(x)* is the vertical deflection, *x* is the location on the beam of the force, and *L, b, h* represent the dimensions of the beam. Appropriate supporting beams should deflect several orders of magnitudes less than the thickness of the NEMS resonating beam. Such minimal deflection will eliminate the possibility of gravitational forces loading the beam.

Adding support beams requires the comb drive to create a greater amount of force. Larger forces can be achieved by increasing the number of fingers.

III. Thermal Time Constant

The resonating beam is heated using a DC voltage. Tuning provides control over the resonant frequency of the beam. The speed at which the frequency of the beam can be tuned is highly dependant on the *thermal time constant*. The thermal time constant of an actuator is the measure of time required for the actuator to cool down to ambient temperature following actuation. It also determines the maximum operating frequency, independent of the resonant frequency.

Solving for the time constant requires the setting of many equations and conditions.

The one dimensional Heat Flow Equation states:

$$\frac{\partial u}{\partial t} - k\frac{\partial^2 u}{dx^2} = \frac{Q(x,t)}{C_p}$$

Equation 15 [5]

With the boundary conditions

$$B.C.(1): u(o,t) = T_w$$
$$B.C.(2): u(L,t) = T_w$$
$$I.C.: u(x,0) = f(x) = T_w$$

Equation 16 [1]

where $Q(x,t)$ is the thermal energy per unit volume per unit time, k is the thermal conductivity, ω_0 is the resonant frequency and $T = \frac{2\pi}{\omega_o}$, and C_p is the specific heat capacity. Applying a direct current gives

$$I = I_0 t$$

Equation 17

$$I^2 = I_o^2 t$$

Equation 18

Using this, as well as integrating the area and thermal energy distribution;

$$\widetilde{Q} = \frac{1}{T}\int_0^T \int_0^L A(Q(x,t))dxdt$$

Equation 19 [1]

gives the result of

$$\widetilde{Q} = \frac{(I_0^2)(R)(\pi)}{\omega_o}$$

Equation 20 [1]

Defining a new function allows for the boundary conditions to be equal to zero:

$$v(x,t) = u(x,t) - T_w$$
$$B.C.(1): v(0,t) = T_w - T_w = 0$$
$$B.C.(2): v(L,t) = T_w - T_w = 0$$
$$I.C.: v(x,0) = T_w - T_w = 0$$

Equation 21 [1]

$\therefore$

$$\frac{\partial v}{\partial t} - k\frac{\partial^2 v}{dx^2} = Q(x,t)$$

$$B.C.(1): v(0,t) = 0$$

$$B.C.(2): v(L,t) = 0$$

$$I.C.: v(x,0) = 0$$

Equation 22 [1]

In order to match the boundary conditions, there must be a combination of plus *and* minus eigenfunctions, thus expanding the eigenfunction equation:

$$v(x,t) = \sum_{n=1}^{\infty} a_n(t)\phi_n(x)$$

$$where \ \phi_n(x) = \sin(\frac{n\pi x}{L})$$

Equation 23 [1]

This is a spatial sinusoid.

The normalization factor is omitted because eigenfunctions of different *n* are always orthogonal. The solutions of the eigenfunction expansion formula gives a set of values known as *Sturm-Liouville Values*. The Sturm Liouville theory states that for a second order ordinary differential equation

$$\frac{d}{dx}\left(p(x)\frac{dy}{dx}\right) + (\lambda\omega(x) - q(x))y = 0$$

Equation 24 [2]

,where λ is a function and $\omega(x)$ is the *weighting function*. The solutions of lambda, with appropriate boundary conditions, and the corresponding *u(x)* solutions are the eigenfunctions. Using the

Initial Condition: $v(x,0) = 0$

$$\sum_{n=1}^{\infty} a_n(0)\phi_n(x) = 0$$

$$\therefore a_n(0) = 0$$

Equation 25 [10]

and the aforementioned heat flow equation provides the generalized Fourier series for *Q(x,t)*:

$$Q(x,t) = \sum_{n=1}^{\infty}(\frac{da_n}{dt} + \lambda_n ka_n(t))\phi_n(x)$$

Equation 26

To solve for the Fourier coefficients, a_n, the equations of orthogonality can be used:

$$\frac{da_n}{dt} + \lambda_n ka_n = \frac{\int_0^L Q(x,t)\phi_n(x)\,dx}{\int_0^L Q_n^2(x)\,dx} \equiv q_n(t)$$

$$where \ Q(x,t) = \sum_{n=1}^{\infty} q_n(t)\phi_n(x)$$

$$(weighting \ function = 1)$$

Equation 27 [1]

,where the numerator is

$$\frac{C_1 L}{n\Pi}(1 + (-1)^{n+1})$$

Equation 28 [1]

and the denominator is simply L/2.
    Thus:

$$e^{\lambda_n kt}(\frac{da_n}{dt} + \lambda_n ka_n) = q_n(e^{\lambda_n kt})$$

Equation 29 [2]

with $e^{\lambda_n kt}$ being the integrating factor thus making the function integratable.

This results in

$$a_n(t) = l(n)e^{-\lambda_n kt}\left(\left(\frac{e^{\lambda_n kt}}{\lambda_n^2 k^2}(\lambda_n kt - 1)\right) + \left(\frac{1}{\lambda_n^2 k^2}\right)\right)$$

$$where \quad l(n) = \frac{C_1 2}{n\Pi}(1 + (-1)^{n+1})$$

Equation 30 [1]

The time associated with the longest time to reach steady state corresponds to the *n*=1 eigenmode. The term that supplies this is

$$e^{-\lambda_n kt}$$

Equation 31 [2]

where

$$\lambda_n = \left(\frac{n\pi}{L}\right)^2 = \frac{n^2\pi^2}{L^2}$$

$$k = \frac{k_0}{\rho C_p}$$

Equation 32 a&b [13]

Thus,

$$\tau = \frac{1}{\lambda_n k} = \left(\frac{n^2\pi^2}{L^2}\right)\left(\frac{\rho C_p}{k_o}\right)$$

Equation 33 [5]

and the result is a thermal time constant equal to 1.69124 * 10^{-7}s.

| Important values for gold			
Thermal conductivity	Density	Specific Heat Capacity	Length
(W/(m*K))	(kg/m^3)	(J/(kg*K))	(m)
148	19300	128	0.00001

We are assuming that most of the structure will be gold and there will be a minimal effect from palladium.

IV. Design Results

The dimensions of the resonating beam and desired compressive and tensile loading are applied as the initial design constraints. The initial dimensions of the beam are assumed to be ~10 *µ*m long, 80 nm wide, and 100 nm thick. Based on a beam loading of 200 MPa, a desired applied force of 1.6 *µ*N can be calculated from equation 1. The effective Young's modulus of a composite gold/palladium beam is found to be approximately 85 GPa. The gold/palladium NEMS beam compresses under such axial loading. As a result, the beam deflects axially by 25.6 nm, which is determined using equation 6.

Through these design requirements of axial force generation and deflection, we have developed a comb drive suspended in space by four support beams. Figure 4 illustrates an accurate layout of the MEMS comb drive electrostatic actuator.
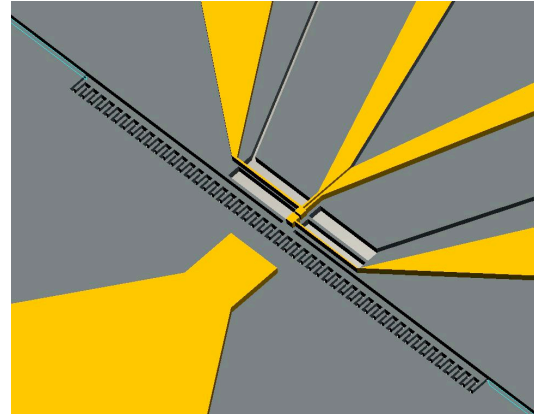
Above view of the MEMS structure
Figure 4

The four-support beams are 50 *µ*m long, 2 *µ*m wide, and 5 *µ*m thick. They are dimensioned to eliminate vertical displacement of the comb drive, beam support block, and the resonating beam itself. Vertical deflection of the cantilevered beams would result in undesirable loading of the resonating beam. Based upon the density of silicon, which is the comb drive and beam support block construction material, and

the density of the gold/palladium composite evaporated onto the silicon, we determined a combined mass of $4*10^{-9}$ kg. Applying Newton's second law to determine a gravitational force, the cantilevered beam deflection equation provides a vertical displacement of 96.7 pm for the entire beam support structure. This vertical displacement of the resonating beam is several orders of magnitude less than the thickness of the beam. Such minuscule deflection is acceptable.

The spring constant of the four identical support beams is determined using equation 10 &11. We determined this spring constant of one individual beam to be 100.8 N/m. Multiplying this value by four for each support beam, a complete spring constant is determined. This combined spring constant along with the known axial deflection of the resonating beam are multiplied, as equations 13 indicates. The result of 10.5 μN is the force necessary to move the entire beam support structure a lateral distance of 25.6 nm. From these calculations, we found the total comb drive force required to be 12.1 μN. Such a force will result in a support block displacement and beam axial deflection of 25.6 nm. In addition, the beam will experience 200 MPa of loading with a comb drive generating 12.1 μN.

The comb drive designed to generate 12.1 μN of lateral force has 50 fingers that are each 8 μm long, 2 μm wide, and 5 μm thick. The overlap between interlocked fingers is 6 μm. Figure 4 also shows a dimensioned view of several fingers of the comb drive system.

Applying the comb drive lateral force generation equation yields the desired force output at an input voltage of 127.99 V. If during experimentation greater or smaller loading is required, a

nearly linear relationship exists between force and input voltage, which is a significant advantage to comb drive electrostatic actuation. This relationship between force and applied voltage is illustrated in figure 5.
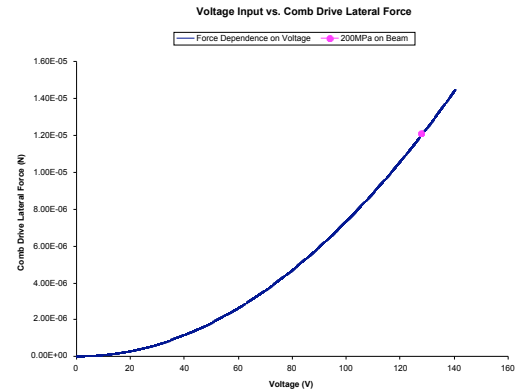
Voltage Input vs. Comb Drive Lateral Force
Figure 5

Similar to force, lateral displacement also maintains almost a linear relationship with input voltage, which is shown in figure 6.
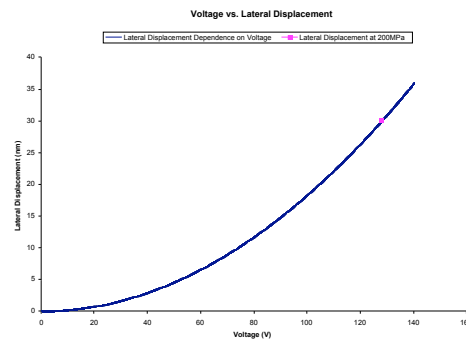
*Voltage vs. Lateral Displacement*
Figure 6

While designing a comb drive system, we also took into account side instability. To ensure that the comb drive network would not experience snap down, the comb drive finger dimensions are such that side instability voltage is 1320 V, which is two orders

of magnitude larger than the working range.

IV. Fabrication

The fabrication starts with a SOI (Silicon on Insulator) wafer. A SOI chip works by placing a thin, insulating layer, such as silicon oxide below the thin silicon wafer. For the purpose of our experiment we will be using a Si-SiO$_2$-Si wafer. This is illustrated in figure 7. The depth of this wafer will 5 μm-1 μm-125 μm, respectively. The processing steps begin with a SIO p-type doped wafer. We use the RCA clean to prepare the wafer and then spin on positive photoresist.
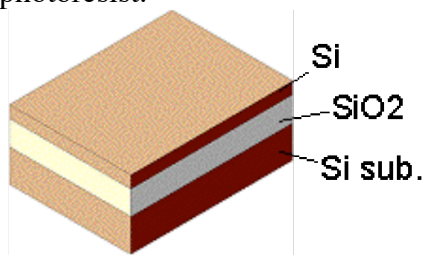
Silicon/Silicon Dioxide/Silicon Wafer
Figure 7

The wafer is then expose using the Mask #1, which is shown in Figure 8. After baking the photoresist and removing the unexposed area, E-beam lithography is used to evaporate the gold/palladium substance. The gold/palladium, due to its insusceptibility to 5:1 BHF etching and high conductivity, is used as the resonating beam and contacts [12]. The photoresist is now lifted leaving only the beam and contact pattern on the surface of the silicon, as can be seen in Figure 8. The wafer is now cleaned for preparation for Reactive Ion Etching.
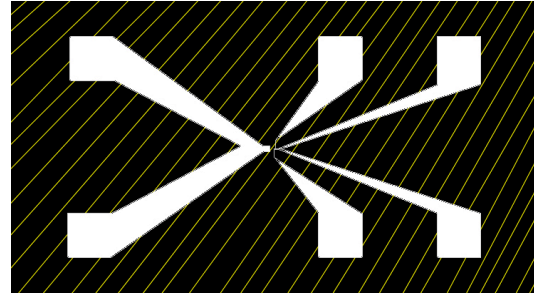

Mask #1: Contact Placement
Figure 8

A positive photoresist is again spun on and developed using Mask #2. Reactive Ion Etching (RIE) is used to vertically etch to the silicon dioxide layer 5 μm below. The RIE process uses low-density diode plasma. This process typically uses a chloride or Bromine based corrosive chemistry with or without fluorine based pre-cursors. This typically leads to lower silicon etch rates of $< 1\mu$m/min giving lower system output. Mask selectivity requires either a hard oxide mask or a thick photoresist. Since it is hard to control beyond 10μm, the structure we etch into is 5μm thick. At a rate of about 1μm/minute, it will take roughly 5 minutes to complete but this variable might change from machine to machine.

Two views of our Mask are shown. Figure 8 shows the far out view of Mask #2, which illustrates where etching exists to form electrically isolated regions. Figure 9 shows the close up view of the mask where the structure will be cut.

Due to the ratio of roughly 100:1 between the depth and resonating beam width, the RIE will remove the silicon under the gold beam. If SEM imagine indicates that the resonating beam was not fully released from its silicon substrate, we will purge the structure with XeF$_2$ gas to etch the thin layer of silicon. Due to the highly reactive nature of the XeF$_2$ etch with silicon, this step would take roughly 5-10 seconds

and must be immediately purged with an inert gas. The beam is now fully released.
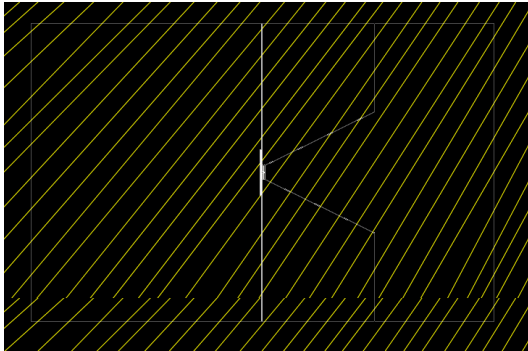
Mask #2: Far Out View
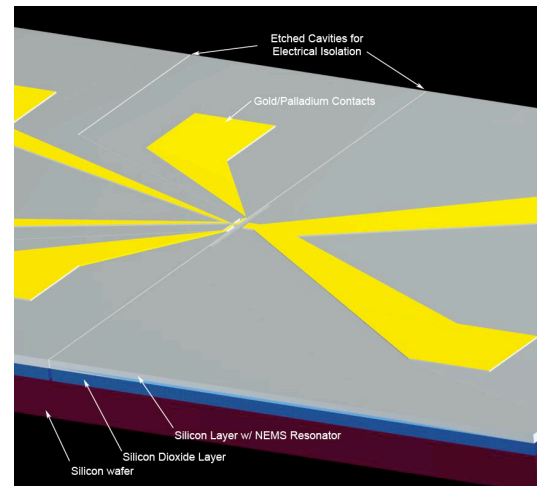**Figure 9**
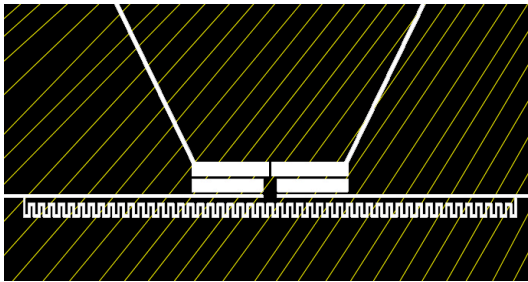
Mask #2: Close Up View
Figure 10

The reason electrical isolation of regions within our design is to enable separate voltage bias to be applied to the comb drive and resonating beam.

In order to release the structure from the wafer, the silicon oxide must be cut. Due to the sensitive nature of silicon and gold, a 5:1 BHF etch is used [12]. This etch will take approximately 30 minutes in order to guarantee the structure being released. Due to the "wet" nature of the etch and the small area between the silicon substrates, supercritical drying must be used to prevent the appearance of water or etchant which could lead to stiction and destroy the structure. Supercritical drying is a process to remove liquid in a precisely controlled way, similar to freeze-drying.

As a substance crosses from liquid to gas, the size of the liquid decreases. As this happens, surface tension at the solid-liquid interface pulls against any structures that the liquid is attached to. Delicate structures such as a MEMS device, tend to break due to surface tension.

In supercritical drying, the route from liquid to gas does not cross any phase boundary, instead passing trough the supercritical region, where the distinction between gas and liquid does not apply.

For the purpose of this step, CO_2 will be used since it is readily available and has a critical point at 31.1°C at 1072 psi.

*Complete structure*
Figure 11

The device is now tested and prepared for mounting and packaging as figure 11 above illustrates.

V. Packaging

In the NEMS and MEMS fields, packaging is often one of the more challenging and limiting components due to size constraints. The integrated NEMS/MEMS sensor expounded upon

requires a complex packaging method that enables complete conductance between the micro-machined device and input/output wires, while also maintaining stability over time and environmental. Moreover, such resonators must be exposed to the mediums under examination in order to detect mass or compute quantum measurements.

While current research experimentation requires a superconducting magnet in a cryostat, successful implementation will involve a smaller, portable magnet and proper functioning under ambient pressure and temperature. With parametric amplification, detection of mass or specific organic compounds is more likely possible. The ideal packaging schematic involves the micro-machined NEMS resonator and MEMS actuator mounted in a leadless configuration onto Pyrex with a protective steel casing, as illustrated in figures 12 [6]. Since all of the applications for such a device have not fully been explored, the packaging will be uniquely tailored for each application. The packaging schematic discussed and illustrated here assumes implementation as a mass detection or organic sensing device.
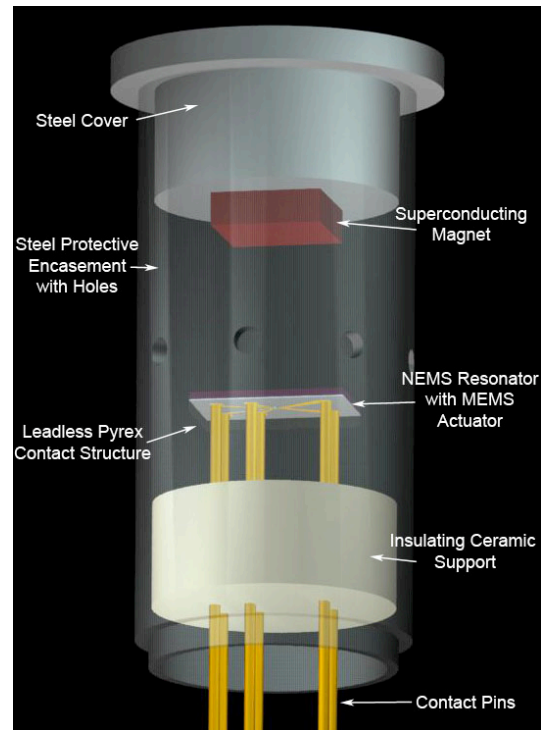

Device packaging
Figure 12

The holes within the steel encasement will allow a flow of the substance under inspection to the sensor. For example, a gas can flow into the steel chamber through these holes and the NEMS/MEMS device could determine if hydrogen is present. The presence of hydrogen would combine with the palladium in the composite gold/palladium beam. Consequently, the lattice structure of the beam would change which would result in a resonant frequency shift. The frequency shift would be detected through the contact pins, and the presence of hydrogen would be known.

The superconducting magnet, which is necessary for the detection of such frequency shifts, will be mounted with epoxy into the steel cover. The steel cover will serve as a protective encasing and a support for the magnet.

The insulating Pyrex structure supports the contact pins onto which the

NEMS/MEMS device will be mounted. This Pyrex piece will be manufactured by powder injection molding. A Pyrex powder will be compressed in a die cavity that possesses the desired shape of the final structure. The piece is then fired into solid Pyrex, and the brass contact pins are sealed into the structure.

The leadless Pyrex contact structure manufactured from a 381 *µ*m Pyrex wafer. This Pyrex piece is a structural support for the NEMS/MEMS device. Holes for the brass pins and a large volume cavity for beam exposure are then drilled with a cavitron into it. Next, the holes of the Pyrex contact structure are aligned with the gold contacts on the micro-machined NEMS resonator wafer. The silicon wafer containing the device is then anodically bonded to the drilled, leadless Pyrex contact structure. The device mounted to the leadless Pyrex structure is illustrated below in figure 13.
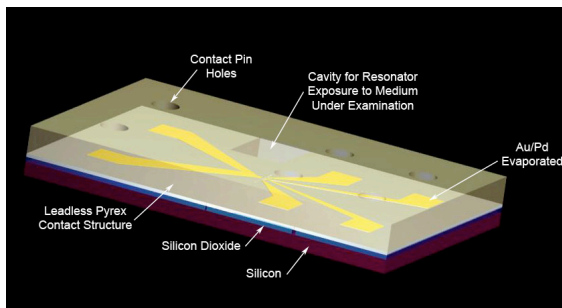

Resonator and actuator mounted on an insulating leadless support.
Figure 13

The pin holes in the Pyrex are then filled with a conductive paste, and the entire leadless setup is mounted onto the brass contact pins protruding through the insulating Pyrex support. The assembly is then heated to harden the paste, which ensures structural stability of the device and excellent conductivity between the brass pins and the

NEMS/MEMS device. A preassembled view is shown in figure 14.
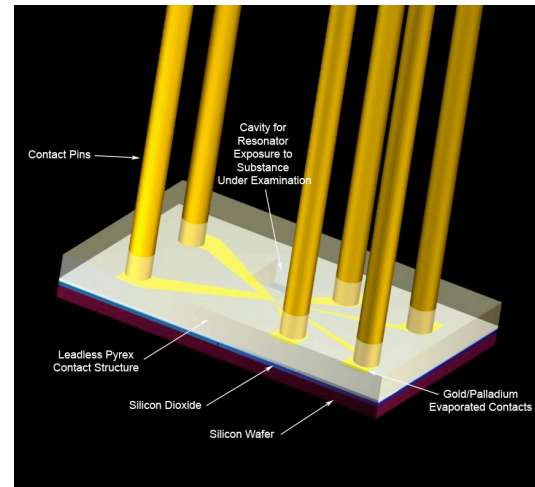
Leadless contact approach
Figure 14

The traditional packaging method would involve ball bonding the contacts in order to create electrical contact between the brass pins and the NEMS/MEMS device. While this method is a well developed industry standard, it has several disadvantages that do not exist within this leadless design. The ball bonding technique entails soldering tiny wires between the gold contacts on the NEMS/MEMS device and the brass pins. These wires are approximately the size of a human hair and easily break under significant vibration. Moreover, ball bonding becomes less reliable at higher temperatures. The leadless design presented forms excellent electrical contact between the NEMS/MEMS device and the brass pins. In addition, its robust contacts eliminate the possibility of losing conductivity in extreme environments, where significant vibration is present.

Many of the applications of this device are related to antiterrorism. Such a device along with this packaging

schematic would be suitable for detecting finite amounts of organic compounds that would naturally be present in explosives. This is a short list of the numerous applications for such a device.

VI. Device Operation

The device works through the use of the LabView program software, which is attached to the contacts. As one might notice from the drawings, there are more contacts then necessary to use the structure in its simplest form. This allows the user to change parameters and different biases to push the designs limits. Also, it allows the user to have grounds and to be able to measure the voltage at the silicon level for active feedback.

The operation of the comb drive structure can be seen in figure 3. A voltage bias is applied to contacts leading to each side of the comb drive. This difference in voltage between the left and right side of the structures actuates the comb. The difference for maximum output has to be a difference of 127.99V.

Due to the fact that beam will be resonating, an AC current must be applied on top of the DC current that places the bias on the comb drive. This is done 180° out of phase from the current applied to the resonating beam. This will be applied through one of the left hand side contacts, using figure 13 as a reference.

The nano resonating beam will be driven magnetomotively by a Lorentz force. The beam's frequency will be tuned by applying a DC bias to the gold contacts attached to the beam. The direct current heats the beam which shifts its resonant frequency downward.

The tuning DC bias can be placed using the upper right two contacts attached to the beam. The middle contacts, which connect to one side of the beam and one side of the comb drive, will both be connected to ground or a reference voltage. The resonant frequency shifts can be measured using a magnetomotive technique [13].

VII. Conclusion

A relationship characterizing the electromechanical behavior of the comb driven structure on the doubly clamped resonating beam has been formed. The model, masks, fabrication steps and calculations have all been derived for ease in manufacturing and packaging. A suggestion for further research would be a feed back loop in order to determine the distance traveled by the block structure. This would most likely be a small electrostatic capacitive parallel plate sensor on the edge of the comb drive. We are currently evaluating alternative approaches to excitation and capacitive detection in order to expand the applicability of the device.

VIII. Acknowledgements

IX. References

[1]Haberman, Richard. <u>Applied Partial Differential Equations</u>. Prentice Hall. 2004.

[2] <u>MathWorld.</u> Stephen Wolfram. March 10, 2005. Wolfram Research, Inc. December 10, 20005. <http://mathworld.wolfram.com/>.

[3] G. Abadal. "Electromechanical model of a resonating nano-cantilever-based sensor for high resolution and high-sensitivity mass detection", Nanotechnology 12 (2001) 100-104.

[4] Z.J. Davis. "High mass and spatial resolution mass sensor based on Nano-cantilever Integrated with CMOS", Transducers'01 Conference Technical Digest, pp72-75 (2001).

[5] Senturia, Stephen D. <u>Microsystem Design</u>. Springer. 2001.

[6] Kulite Semiconductor Products Inc. (2005) Apparatus And Method For Interconnecting Leads In A High Temperature Pressure Transducer. US patent number 6,895,822 B2. May 24, 2005.

[7] MEMS class. Fall 2005. Prof. Chee Wei Wong. Columbia University. Lecture 7.

[8] Rob Legtenber, A W Groeneveld and M Elwenspoek. "Comb-drive actuators for large displacement." J. Micromech. Microeng. 6 (1996) 320-329.

[9] Ki Bang Lee, Liwei Lin. "Vertically supported two-directional comb drive." J. Micromech. Microeng. 15 (2005) 1439-1445.

[10] Michael Mendalaous, Graduate Student, Mechanical Engineering. Columbia University.

[11] Tam Pandhumsopron. "High etch rate, deep anisotropic plasma etching of silicon for MEMS fabrication" Alcatel Vacuum Technology.

[12] Kirt R. William. "Etch rates for micromachining processing – Part II." Journal of Microelectromechanical systems, Vol. 12, No.6, December 2003.

[13] James Hone. "Electrothermal tuning of composite Al-SiC nanomechanical resonators."

X. Biography

Adam Hurst recently received his Bachelors of Science in Mechanical Engineering from Columbia University. He is currently working at Kulite® Semiconductor Products as a design and development engineer. In addition, he is working on his Master of Science degree at Columbia University. He also likes to run and climb walls with Prof. Hone.

Chou Ying-Chi is currently a graduate student in department of Mechanical Engineering at Columbia University. He received his Bachelors of Science from Tamkang University where he studied Mechanical Engineering.

John Regis has received his Bachelor of Science degree in Physics from Adelphi University, as well as his Bachelor of Science degree in Mechanical Engineering from Columbia University in 2003 and 2005, respectively. He is currently a 1st year graduate student in the department of Mechanical

Engineering at Columbia University. Some of his research interests include: Controls, Manufacturing, and Product Design/Analysis. After getting his Master's degree, he will seek employment at an engineering company where he can work exclusively on manufacturing and product design.

Andrew Lie is currently a senior undergraduate student in the Department of Mechanical Engineering at Columbia University. Upon graduating, he will be working as a strategy consultant for Accenture in California while pursuing his Silicon Valley start-up company.

Adrian Podpirka is currently a senior undergraduate engineering student in the Department of Material Science at Columbia University pursuing a Bachelors of Science. At the moment, he is applying to graduate school where he hopes to continue his studies and work towards a doctorate degree in Material Science. His research interests include fuel cell membranes and semiconducting materials. He is also a four-year member of the varsity lightweight crew team.